JOURNAL OF MATERIALS SCIENCE **40** (2005) 6011 – 6017

Morphology and structure of airborne β-SiC fibres produced during the industrial production of non-fibrous silicon carbide

A. E. GUNNÆS*, A. OLSEN
Department of Physics, University of Oslo, Centre for Materials Science and Nanotechnology, Gaustadalleen 21, NO-0349 Oslo, Norway
E-mail: eleonora@fys.uio.no

A. SKOGSTAD, E. BYE
National Institute of Occupational Health, Department of Occupational Hygiene, PO Box 8149, NO-0033 Oslo, Norway

Clusters of airborne SiC fibres from the SiC industry have been studied by scanning and transmission electron microscopy (SEM, TEM). These fibres are produced as an unwanted side product during the industrial manufacturing of non-fibrous silicon carbide. It was found that the complex morphology seen for clusters of SiC fibres can be explained on the basis of the crystal structure of the fibres. By use of electron diffraction (ED) and high resolution electron microscopy (HREM) it was found that the SiC fibres can be described as needles based on face centred cubic structure (space group $F\bar{4}3m$ and $a = 0.4385$ nm). The needles are covered by a thin amorphous layer of carbon. The needles contain a high degree of stacking faults and twinned areas. No long-range order of a hexagonal structure as a result of stacking faults was found.

The SiC needles grow along the $\langle 111 \rangle$ directions. The existence of equivalent $\langle 111 \rangle$ directions in the cubic structure, separated by an angle of 70.52°, explains the most common angle found between branches and the parent needle. Single and double twinned areas in the cubic structure have been found to produce a second and third set of angles between branches and a parent needle. The second set of angles is 38.94°, 43.31°, 55.53°, 56.25° and 66.16°. One example from the third set is the angle ~83° (~97°). These parent needles with branches may be significant to the toxicological effects of the airborne SiC fibres.

1. Introduction

A large number of reports related to SiC fibres/whiskers can be found in the literature as SiC fibres are commonly used as reinforcement in different alloy systems. However, the interest in SiC fibres in the present work is related to the fact that it has been reported that airborne SiC fibres occur in SiC manufactory plants using the Acheson process [1–3]. The Acheson process, which is one type of the carbothermal reduction method, is the most common process for production of SiC. The SiC fibres are unwanted side products of this non-fibrous SiC production and are considered as pollutants. Recent epidemiological studies have shown association between exposure to airborne dust and lung and stomach cancer and other lung diseases in this industry [4, 5]. It is of great importance to identify the risk factors for the increased incidence of cancer and other lung diseases among the workers in the SiC industry. SiC fibres are likely candidates although the existing epidemiological evidence cannot differentiate between different dust components. The identification of specific particles would provide us with a better potential to assess the excess health risk and more important the possibility for preventive actions directed towards the sources of the risk factors. A prerequisite for this is a reliable method for assessment of specific fibre type exposure among the workers. Evaluation of the risk associated with the fibre exposure is dependent on the assessment of the fibre concentration in the workplace atmosphere. The size and geometry of the fibres are essential for both the toxicity and the visibility of the fibres in the microscope. The concentration of airborne particles is accepted as a valid indicator of the inhaled dose. The standard WHO-method for counting asbestos is developed for single fibres [6]. However, these counting rules are not easily applied for clustered SiC fibres, seen to a large extent in the air samples. Several topics have to be sorted out in the search for an improved fibre counting

*Author to whom all correspondence should be addressed.
0022–2461
DOI: 10.1007/s10853-005-4591-y

procedure. First of all the chemical composition and the morphology of all the fibre types have to be determined.

Although SiC has a simple chemical formula it is known to have more than 150 different polytypes [7]. All SiC structures are made up of a single basic unit, a layer of tetrahedra (SiC_4 or CSi_4). The polytypes are usually represented by a number indicating how many SiC_4 (or CSi_4) tetrahedra that are stacked along the $[001]_{hex}$ or $\langle 111\rangle_{cub}$ direction in the unit cell and a letter indicating the crystal symmetry (C-cubic, H-hexagonal and R-rhombohedral) [8]. The cubic 3C structure is generally referred to as β-SiC whereas the hexagonal and rhombohedral structures are referred to as α-SiC.

The condition under which SiC is formed in the Acheson process is not easily recorded. In this process large batches are made in huge open industrial furnaces where unreacted materials from previous runs can be reused in new batches. The final SiC product undergoes a secondary process where β-SiC is transformed to α-SiC. Airborne SiC fibres have been reported to consist of various fibre types [1–3]. A large variety of airborne SiC fibres was also seen by the present authors, however the aim of the present study was to investigate clustered SiC fibres in order to get more insight about their chemical composition, structure, surface properties and morphology. With more knowledge of the clusters a better quantification procedure for clustered SiC fibres may be developed based on the existing WHO-method for counting asbestos [6].

2. Materials and methods

The SiC fibres studied in the present investigation were collected from one of three industrial SiC plants in Norway. In these plants SiC is produced in Acheson resistance furnaces where mixtures of petroleum coke and quartz/silica sand are heated up by a core of compact graphite. The core forms a resistor where the electric energy is supplied for a period of about 65 hours. In the process particles of quartz (SiO_2) and coke (C) can react and produce SiC at contact areas at lower temperatures. Above 1520°C SiO_2 transform to O_2 and SiO gas. SiO can diffuse to coke particles where it reacts with the coke and produces solid SiC and CO gas. Primary SiC is first produced close to the centre of the core where the temperature is highest. The reaction proceeds outwards as the temperature increases from the core. The primary SiC produced is known to have cubic crystal structure (β-SiC). As the temperature increases above 2000°C the β-SiC starts to sublimate and Si-rich gas diffuses out towards cooler areas in the furnace and reacts with free C and partly with CO. SiC produced in this secondary process has the desired α-SiC structure. When the heating cycle has ended the result is a SiC ingot (crude) grading 85–100% SiC and a quantity of unreacted material that can be used in a new batch. The highest purity material is found close to the core and the impurity level is increasing outwards. The outer area of the ingot consists of fine grains of SiC and is referred to as firesand.

2.1. Collection of furnace samples

After completion of a heating cycle and dismantling of the furnace, fibre-containing material was collected from the zone between the SiC crust and the outer firesand layer. The material was dispersed in ultra-pure H_2O and centrifuged. After 3 subsequent washings, 5–10 μl of the suspension was applied on 200 mesh Ni grids with lacey carbon film and air-dried.

2.2. Collection of air samples

Air samples were collected by personal sampling in the furnace hall. Twenty five mm polycarbonate filters (PC) were applied with pore size 0.4 μm using open-faced graphite-filled 25 mm filter holders with 50 mm extension tube (Gelman Air Monitoring Cassette, Gelman Sciences, Ann Arbor, MI, USA). The airflow through the filter was adjusted to 1 liter min^{-1} using pulsation-free battery-powered pumps constructed at NIOH (National Institute of Occupational Health, Oslo, Norway).

2.3. SEM and TEM sample preparation

The exposed polycarbonate filters were transferred to clean glass beakers. The inside of the corresponding cassette cowl was rinsed with 10 ml of 25% ethanol and the liquid was collected in the glass beaker with the filter. The filter with the rinsed liquid was sonicated for 3 min. in an ultrasonic bath to liberate the particles from the filter. Two sub-volumes from the homogenized particle suspension, each of 3 ml, were filtered using a funnel with a 15 mm internal diameter on each of the following filters: (1) PC filters coated with a 100 nm layer of platinum and an effective pore size of 0.2 μm for SEM analysis and (2) uncoated PC filters with pore size 0.2 μm for TEM analysis. Filters for SEM analysis were cut and pieces with size 6×6 mm were mounted on aluminium specimen stubs with double-sided carbon adhesive discs and with additional spots of carbon cement at each corner to secure good conductivity to earth. The samples were coated with a 10–15 nm platinum layer in a Balzers SCD 050 sputter coater (Balzers, Liechtenstein). Additional samples without coating were also prepared. Filters for TEM analysis were prepared as follows: Half of the filter (2) was mounted on clean glass slides with pieces of tape and coated with approximately 50 nm carbon film in a high-vacuum thermal evaporator (Jeol JEE 4×). Pieces of 4×4 mm were cut from the coated filter, mounted on 200 mesh Cu-grids and digested in chloroform overnight in a Jaffe-washer [9].

2.4. SEM and TEM analysis

A combination of scanning and transmission electron microscopy (SEM and TEM) was used to study the SiC fibres. A Jeol JSM-6400 equipped with a Vantage DSI energy dispersive X-ray spectrometer (EDS)-system with a thin window detector was used in the SEM investigation. The SEM was operated with an acceleration voltage in the 5–20 kV range. A JEOL2000FX TEM operating at 200 kV was used for diffraction and low

magnification microscopy whereas a JEOL2010F TEM equipped with a VANTAGE DI+ analysis system and a Pioneer X-ray detector was used for high resolution imaging of the SiC fibre structure as well as for light element spectroscopy.

3. Results

The different morphologies of SiC fibres found in the air samples were also seen in the samples taken from the furnace. Both sample types were found to have a large variety of SiC fibres. The fibres were different in both morphology and size and were found both as single as well as clusters of fibres. The samples from the furnace differed from the air samples with respect to the amount of larger SiC crystals, which were higher in the furnace sample.

Three different categories of fibre clusters were found in the present study. These can be described as needles with: (a) uneven surface and with one or several branches growing from the 'parent' needle (Fig. 1), or as needles with smooth surface that are either (b) curled or (c) straight with branches (Fig. 2). The SiC clusters in category (a) and (c) consist of needles with branches,

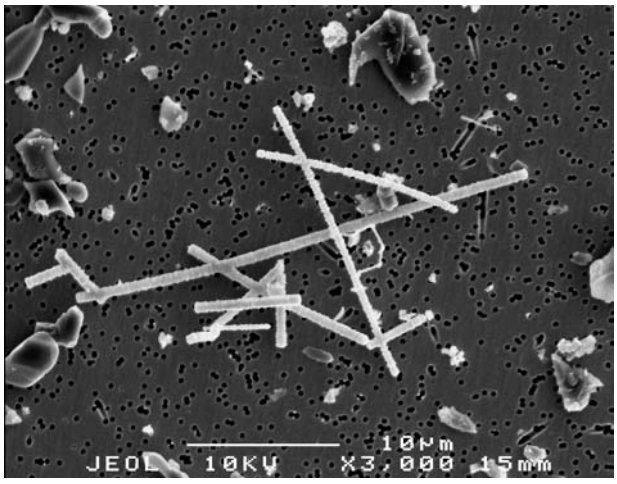

Figure 1 SEM image of a cluster of large SiC needles with branches.

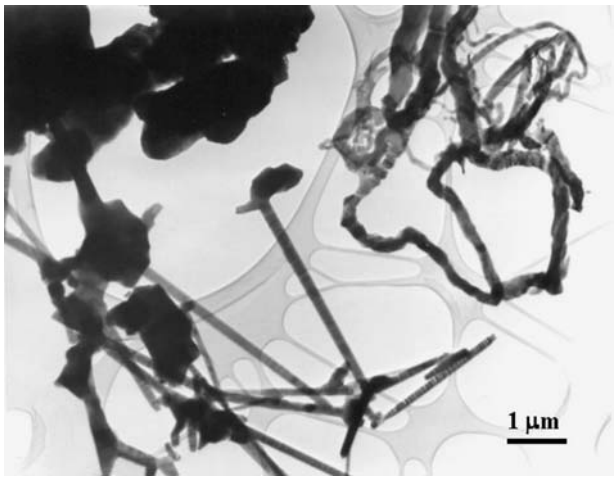

Figure 2 Clusters of thin SiC needles that are curled or straight with branches.

with a specific orientation relative to the parent needle. Due to the depth of focus in the electron microscopy images it is difficult to decide whether the parent needle and its branches are lying in or come out of a plane normal to the incident electron beam. The apparent angle between a branch and its parent needle where one or both of them are going out of this plane, can be under- or over-estimated depending on their orientation relative to the plane. It is therefore vital that both the needle and the branch of interest are lying parallel to the image plane in order to measure a correct value of the angle. This can be achieved by tilting the sample around two axis in the TEM.

By studying single needles lying flat in the TEM specimen holder it was found that the needle axis could be described in the cubic or hexagonal axial system as parallel to ⟨111⟩ or [001], respectively. In order to measure the angle between a needle and a branch, the sample was tilted so that the $\langle 111 \rangle_c / [001]_h$ direction of both the needle and the branch was parallel to the image plane. This can be achieved by first tilting the needle so that the systematic row of 111/001 reflections (parallel to the needle axis) appears in the selected area diffraction (SAD) pattern. The sample should then be tilted around the needle axis keeping the row of systematic reflections in symmetrical orientation until the second 111/001 systematic row of reflections, parallel to the branch, comes in symmetrical orientation. At this point both the needle and the branch will obtain their maximum length and be oriented parallel to the image plane. The angle between the needle and the branch can then be measured directly in the bright field (BF) image or SAD pattern. By following this procedure in the TEM it was found that the branches grow with several angles relative to the needle. However, these angles are not random. The most common angle is ∼70° (∼110°), but ∼39° (∼141°), ∼56 (∼124°) and ∼83° (∼97°) also occur often. Fig. 3a shows an image of the intersection of four needles marked A, B, C, and D of which all except needle D are parallel to the image plane. Needle A and C have the same orientation, and found to make an angle of ∼70° and 110° relative to needle B, respectively. The corresponding SAD pattern is shown in Fig. 3b where one can see the 111/001 row of reflections running parallel to the needle axis. Fig. 4 shows a cluster where all needles are lying approximately parallel to the image plane. The angles were measured from the SAD patterns from the intersections (Fig. 5) and the angles were found to be ∼97°, ∼83°, ∼39° and ∼56°, representing some of the common angles seen between a SiC needle and its branches.

SiC fibres generally show a line-contrast seen perpendicular to the fibre axis. This type of contrast is well known for SiC fibres and is attributed to stacking faults in the structure [7]. The stacking faults also express themselves as diffuse streaks running parallel to the direction of the needle axis in the SAD patterns. Fig. 6 shows two typical SAD images from a SiC needle. The projection shown in Fig. 6a is the projection commonly seen when a single fibre is lying flat in the specimen holder and the holder is not tilted in the TEM. The pattern can be indexed in agreement with the

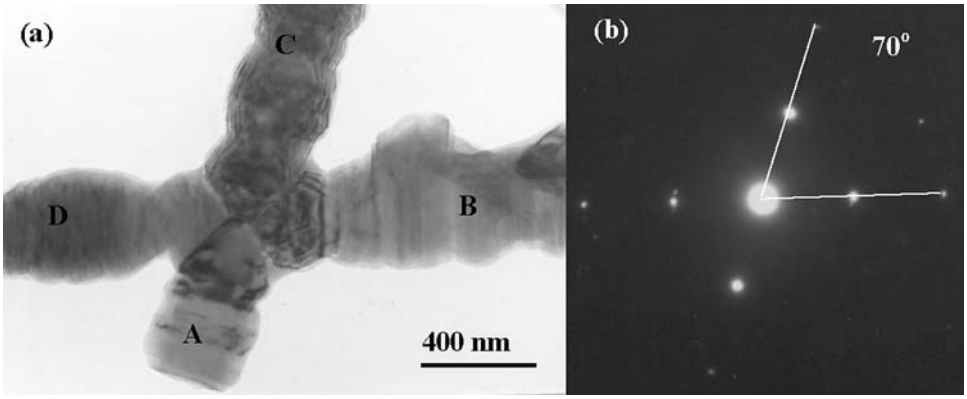

Figure 3 (a) BF image of an intersection of four SiC needles where needle A, B, and C are lying parallel to the image plane. (b) ⟨111⟩ rows of reflections with an angle of ∼70° (∼110°) between needle B and C as seen in the SAD pattern.

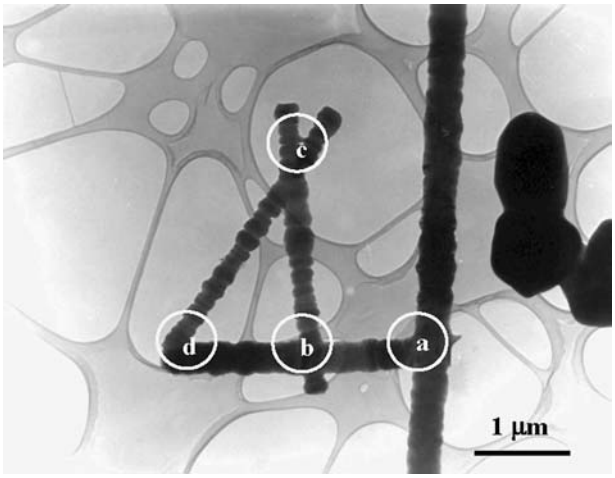

Figure 4 Cluster of SiC needles where all needles/branches are approximately parallel to the image plane.

$[1\bar{1}0]$ projection of all the hexagonal SiC structures as well as the [112] projection of the cubic 3C structure. Fig. 6b shows another projection after tilting around the $111_c/001_h$ row of reflections in Fig. 6a. However, the reflections seen in Fig. 6b can only be indexed in agreement with a ⟨110⟩ projection of the cubic 3C structure (β-SiC). The 3C structure has the cubic space group $F\bar{4}3m$ and cell dimension $a = 0.4385$ nm [10]. The extra reflections seen on the diffuse streak in Fig. 6b can be explained as reflections coming from ⟨111⟩ twins in the cubic structure. The twins can be described as 180°-rotation twins or mirror twins with {111} twinning planes because ⟨111⟩ are 3-fold axes and {110} are mirror planes in the structure.

Fig. 7 shows a HREM image from a SiC needle in a $[1\bar{1}0]$ projection where areas with A, B, C, A, B, C,.. stacking sequence can be seen together with stacking

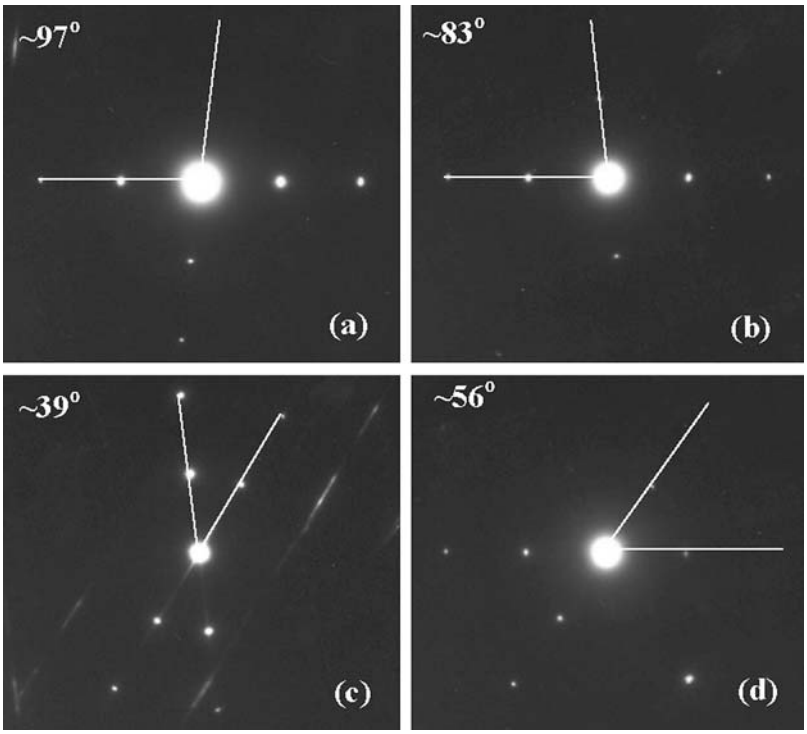

Figure 5 SAD patterns from Fig. 4 showing the angles (a) ∼97°, (b) ∼83°, (c) ∼39° and (d) ∼56° between the ⟨111⟩ rows of reflections.

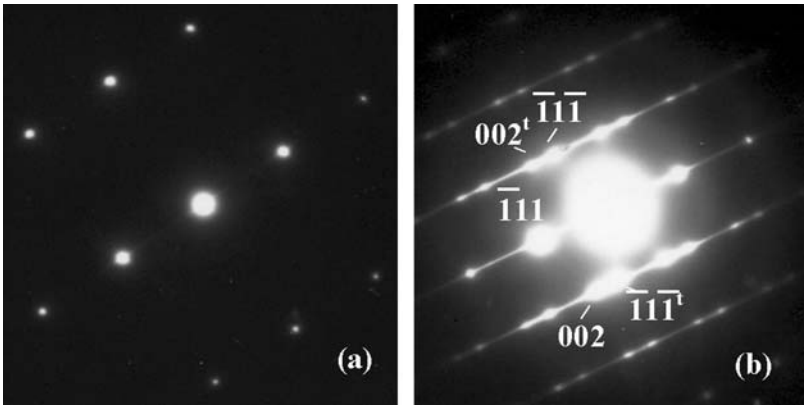

Figure 6 Typical SAD patterns from the SiC needles which can be indexed as (a) the [1$\bar{1}$0] projection for the hexagonal SiC structures or [112] projection of cubic 3C structure and (b) [110] projection of the cubic 3C structure.

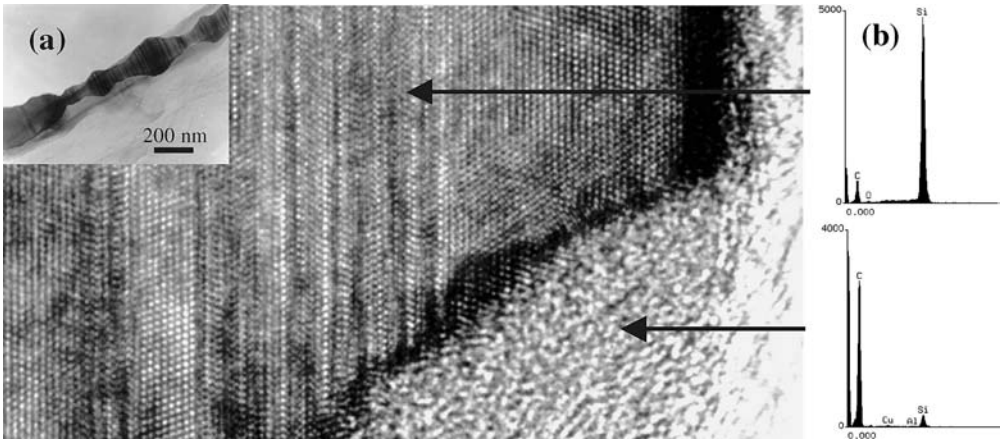

Figure 7 (a) HREM image from a SiC needle showing stacking faults together with the cubic structure and twinned areas. (b) EDS analysis shows that the amorphous layer on the SiC needle is carbon-rich.

faults where the periodicity no longer exists. The stacking faults perpendicular to the needle axis can result in local hexagonal structure, but no hexagonal long-range order was generally found in the present study.

By use of HREM it was found that the SiC needles and its branches have an amorphous surface layer (Fig. 7). The amorphous layer seen in Fig. 7a was analysed by EDS and found to consist mainly of carbon (Fig. 7b). The thickness of the carbon-layer on the needles was generally found to be uniform with exception of the tip of the needles where it was found to be thinner. On some larger elongated SiC crystals with sharp edges, it was found that the thickness of the carbon-layer depends on the type of crystal surface/facet. The crystal shown in Fig. 8 has been imaged in a [01$\bar{1}$] projection and facets corresponding to (100), (111) and (311) planes can be seen. The thickness of the carbon-layer was found to be ∼50 nm thick on the facets corresponding to {100} planes and only a few nm thick on the other facets. At the tip of the crystal, enlarged in Fig. 8b, the starting point of a needle can be seen with characteristic contrast from {111} stacking faults as indicated by arrow. The thickness of the carbon-layer is diminishing towards the tip of the needle.

As for the straight SiC needles the thin curled SiC fibres were found to have the 3C structure with a high degree of stacking faults and twinned areas, see Fig. 2. In contrast to the straight needles, the curled fibres show no clear growth directions. However, evidence has been found that the fibres do not grow in random directions. Fig. 9 shows an example of a SiC fibre that has grown in zigzag but still propagates in the ⟨111⟩ direction similarly to the straight SiC needles. The SAD pattern from the zigzag shaped needle shows clear indication of twinning (Fig. 9). The angle between the local growth directions and the propagation direction (⟨111⟩ direction) in Fig. 9 is close to 70°.

4. Discussion

The SiC needles were found to grow along the ⟨111⟩ direction according to a cubic axial system in agreement with previous reports on β-SiC needles/whiskers/nanorods in the literature [11–16]. Four equivalent {111} planes exist in the cubic structure. This implies that the needle can grow in four different equivalent ⟨111⟩ directions relative to the same crystal unit in the cubic system. The angle between these directions is 70.52° (or 180°–70.52°). This angle is in agreement with the most common observed angle between a needle and a branch in the present study and the observations of [15] reporting on branching phenomena in SiC whiskers. The additional growth angles found in the present study, but not reported by [15] must, however, come from a different crystallographic relationship between the branch and the main needle.

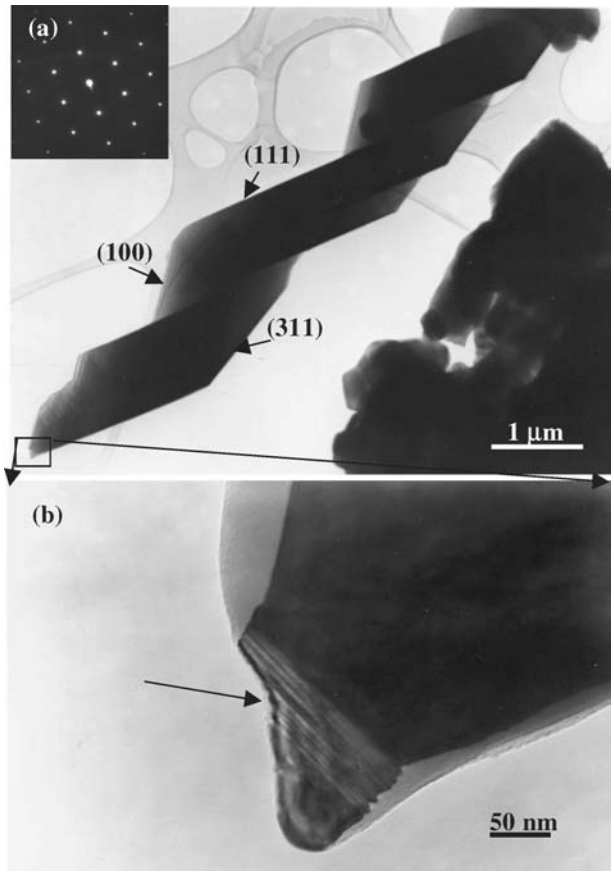

Figure 8 (a) Large elongated SiC crystal with facets and corresponding SAD pattern. The thickness of the amorphous carbon-layer depends on the type of facets. (b) Close up of the tip of the crystal with the starting point of a needle.

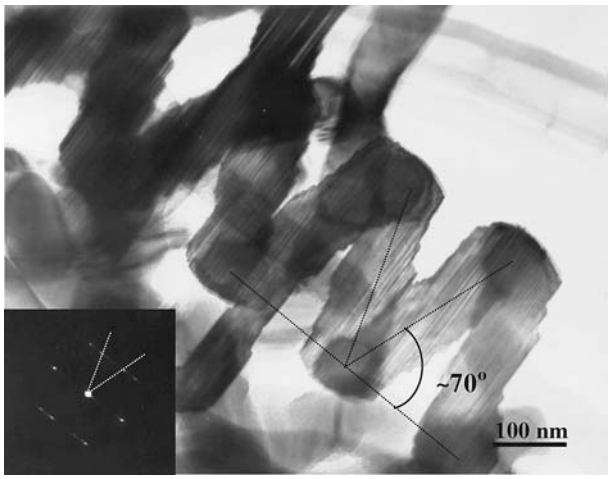

Figure 9 SiC fibre in a curled cluster showing growth propagation in the ⟨111⟩ direction and SAD pattern with clear indication of twinning.

It was found from SAD and HREM that the needles contain numerous stacking faults and twinned area. Stacking faults and twinned areas are frequently reported in SiC needles/whiskers grown by different mechanisms [11, 14, 17, 18]. If a branch starts to grow from a twinned area a set of new angles between the needle axis and the branch axis appear. If the needle axis is defined as parallel to the [111] direction a new set of possible growth directions can be defined in a twinned area. These directions are of the type ⟨115⟩ and ⟨117⟩ when related to the un-twinned structure. Table I summarises calculated angles between the new set of possible growth directions from a twinned area and the [111] direction. As can be seen from Table I the majority of the angles found between the branches and a needle fit very well with the calculated angles between the parent needle and a branch growing from a twinned area in the needle.

TABLE I Possible growth directions and angles relative to a SiC needle with growth axis [111]

Growth directions	[115]	$[\bar{1}15]$, $[1\bar{1}5]$	$[11\bar{5}]$,	[117],	$[\bar{1}17]$, $[1\bar{1}7]$	$[11\bar{7}]$,
	$[\bar{1}\bar{1}\bar{5}]$	$[\bar{1}1\bar{5}]$, $[1\bar{1}\bar{5}]$	$[\bar{1}\bar{1}5]$	$[\bar{1}\bar{1}\bar{7}]$	$[\bar{1}1\bar{7}]$, $[1\bar{1}\bar{7}]$	$[\bar{1}\bar{1}7]$
Angle with [111]	38.94°	56.25°	70.53°	43.31°	55.53°	66.16°

The angle ∼83° (∼97°) seen in the two cases in the cluster shown in Fig. 5 can not be explained on the basis of a single twinned area. However, with the understanding of the other angles seen in Fig. 5, the angle ∼83° (∼97°) can be directly explained. Considering the angles between the needles making a triangle in Fig. 5, two of the angles are due to single twins and the third angle ∼83° (∼97°) can therefore be described as the result of a double twin.

In a hexagonal crystal system there is only one ⟨001⟩ direction and therefore no other equivalent growth directions exist. The growth direction of the branches of a SiC needle can thus not be explained with respect to a hexagonal structure, but can be understood in relation to the cubic structure of the needles.

The observation of cubic β-SiC is not in agreement with previous reports on airborne SiC fibres [1, 2]. In the present investigation the same type of fibres seen in the air samples was also found in the furnace samples taken from the outer part of the ingot. In the outer part of the ingot the temperature has been much lower than closer to the core where SiC has been transformed to α-SiC, and it is therefore not surprising that the airborne fibres found in the present investigation have the cubic structure.

The growth mechanism of the fibres has not been of prime interest in the present investigation. However, the high twinning concentration in the airborne SiC fibres may be related to the increased level of impurities in the outer part of the ingot when the fibres were grown. From studies of SiC whiskers/fibres produced in a carbothermal reduction system where fibres have been grown by vapor-solid (VS), two-stage growth (TS) and vapor-liquid-solid (VLS) mechanism it has been reported that the stacking fault density in β-SiC fibres increases with decreasing diameter [18]. This is in agreement with what is seen in Fig. 8 where the thin tip of the fibre has stacking faults whereas no stacking faults are seen in the thicker part. According to the axial next nearest-neighbour Ising (ANNNI) model [17, 19], stacking faults reduce the energy of the SiC fibres. Formation of stacking faults promotes {111} facets, which have a much lower surface energy than {211} and {110} facets and reduces the total surface energy of the fibres [17].

One can assume that the condition under which the airborne SiC fibres grow in the outer part of the ingot is not stable as heat and gasses are transported out towards the surface of the ingot during the process. Due to unstable growth conditions and increased impurity level it is not surprising that one finds a large variety of SiC fibre that can be very complex in morphology. From the morphology of the tip of the SiC fibres in the clusters one can assume that the clusters have grown by a VS mechanism rather than by a VLS mechanism where one generally finds a droplet shaped tip.

Amorphous layers on SiC needles/whiskers/nanorods have been reported previously [11, 13, 16, 20]. Both carbon and SiO_2 are identified as amorphous on the SiC surface. It is not known whether the amorphous carbon seen on the surface of the SiC needles is vital for the growth process. Amorphous carbon exists in the firesand and it might be assumed that it can cover the SiC fibres without being vital for the growth process. The difference in thickness of the carbon-layer may be related to the number of dangling bonds on the different atomic planes in the SiC structure. However, this has not been investigated further as it is outside the scope of the present study.

5. Conclusion

The complex needle structure seen for some clusters of SiC can be explained on the basis of the cubic crystal structure of SiC. By use of electron diffraction and high resolution electron microscopy it was found that the structure of the SiC needles can be described as face centred cubic with space group $F\bar{4}3$ m and cell dimension 0.4385 nm. The needles contain a high degree of stacking faults and twinned areas that can be caused by impurities in the SiC structure and/or as a result to lower the surface energy of the needle. No long-range order of hexagonal structure was found as a result of the stacking faults.

The SiC needles were found to grow along the ⟨111⟩ directions. The existence of equivalent ⟨111⟩ directions in the cubic structure, separated by an angle of 70.52°, explains the most common angle found between branches and a parent needle. Single twinned areas in the cubic structure have been found to produce a second set of common angles between branches and a parent needle (38.94°, 43.31°, 55.53°, 56.25° and 66.16°). It has also been found that double twinned areas give a third set of possible growth directions relative to the parent needle. One example is the angle ∼83° (∼97°).

The SiC needles were found to have an amorphous carbon-rich outer surface. On larger SiC fibres the thickness of the carbon-layer depends on the type of surface atomic plane.

In the hexagonal crystal system no equivalent growth directions exist for the ⟨001⟩ direction. The complex structure of the SiC clusters can thus only be understood in relation to the cubic structure of the SiC needles.

To what extend the present findings on crystal growth, morphology and the characteristics of the clusters of SiC fibres are important for the observed health effects during the production of non-fibrous SiC is not known. However, we do hope that this description of the chemical and physical properties of this fibrous material may contribute a better insight into the biological mechanism exerted.

Acknowledgments

This investigation was made possible by funds provided by The Bureau of Communities and Regional Affairs (The Norwegian Government) and The Confederation of Norwegian Business and Industry Work Environmental Fund. The authors would like to thank Ole Tormod Fure, The Safty, Health and Environmental Secretariat for the Norwegian Smelters for strong support and constructive ideas during the initiation of the project, and Orkla Exolon KS for good cooperation. Further we thank Per Ole Huser and Kristian Kruse, The National Institute of Occupational Health (NIOH) for carrying out the fieldwork and Bjørn V. Johansen, The Norwegian Public Health Institute for help and discussion on the TEM preparation techniques. Wijnand Eduard (NIOH) is highly acknowledged for valuable discussions and comments on the manuscript.

References

1. E. BYE, W. EDUARD, J. GJØNNES and E. SØRBRØDEN, *Scand. J. Work Environ Health* **11** (1985) 111.
2. A. DUFRESNE, G. PERRAULT, P. SÉBASTIEN, A. ADNOT and M. BARIL, *Am. Ind. Hyg. Assoc. J.* **48** (1987) 718.
3. G. SCANSETTI, G. PIOLATTO and G.C. BOTTA, *Ann. Occup. Hyg.* **36** (1992) 145.
4. C. INFANTE-RIVARD, A. DUFRESNE, B. ARMSTRONG, P. BOUCHARD and G. THERIAULT, *Am. J. Epidem.* **140** (1994) 1009.
5. P. ROMUNDSTAD, A. A. ANDERSEN and T. HALDORSEN, *Am. J. Epidem.* **153** (2001) 978.
6. WHO, 1997, Determination of airborne fibre number concentrations. A recommended method, by phase-contrast optical microscopy (membrane filter method). *World Health Organization*, Geneva.
7. P. T. B. SHAFFER, *Acta Cryst.* **B25** (1969) 477.
8. L. S. RAMSDELL, *Amer. Min.* **32** (1947) 64.
9. International Organization for Standardization. ISO 10312: Ambient air—Determination of asbestos fibres—Direct-transfer transmission electron microscopy method, 1995.
10. N. W. THIBAULT, *Amer. Min.* **29** (1944) 249.
11. G. MCMAHON, G. J. C. CARPENTER and T. F. MALIS, *J. Mater. Sci.* **26** (1991) 5655.
12. S. M. PICKARD, B. DERBY and E. A. FEEST, *ibid.* **26** (1991) 6207.
13. J. ZHU, X. G. NING, H. G. XU, K. Y. HU, W. CAO and H. Q. YE, *ibid.* 26 (1991) 3202.
14. H. WANG, Y. BERTA and G. S. FISCHMAN, *J. Am. Ceram. Soc.* **75** (1992) 1080.
15. Y. C. ZHOU, X. CHANG, J. ZHOU, F. XIA and C. H. SHIH, *J. Mater. Sci. Lett.* **11** (1992) 891.
16. Y. ZHANG, N. L. WANG, R. HE, X. CHEN and J. ZHU, *Sol. State Comm.* **118** (2001) 595.
17. L. WANG, H. WADA and L. F. ALLADR, *J. Mat. Res.* **7** (1992) 148.
18. H.-J. CHOI and J.-G. LEE, *Ceram. Int.* **26** (2000) 7.
19. C. CHENG, R. J. NEEDS and V. HEINE, *J. Phys.* **C21** (1988) 1049.
20. G. W. MENG, L. D. ZHANG, C. M. MO, F. PHILLIPP, Y. QIN, H. J. LI, S. P. FENG and S. Y. ZHANG, *Mater. Res. Bull.* **34** (1999) 783.

Received 15 January 2004
and accepted 16 February 2005